Characterization of Microvascular-Based Self-healing Coatings

K.S. Toohey · N.R. Sottos · S.R. White

Abstract A protocol is described to assess self-healing of crack damage in a polymer coating deposited on a substrate containing a microvascular network. The bio-inspired coating/substrate design delivers healing agent to cracks in the coating via a three-dimensional microvascular network embedded in the substrate. Through capillary action, monomer flows from the network channels into the crack plane where it is polymerized by a catalyst embedded in the coating. The healing efficiency of this materials system is assessed by the recovery of coating fracture toughness in a four-point beam bending experiment. Healing results for the microvascular networks are compared to data for a coating containing microencapsulated healing agents. A single crack in a brittle epoxy coating is healed as many as seven times in the microvascular systems, whereas microcapsule-based healing occurs for only one cycle. The ability to heal continuously with the microvascular networks is limited by the availability of catalyst in the coating.

Keywords Self-healing · Coating · Microvascular · Substrate · Fracture toughness · Autonomic

Introduction

Previous approaches to self-healing polymers include micro-encapsulation of healing agents, hollow fibers, and remendable systems. In capsule-based healing systems [1–8], a liquid monomer is encapsulated by a polymer shell and the microcapsules are dispersed along with solid-phase catalyst throughout the matrix. A similar self-healing approach incorporates hollow fibers that contain epoxy resin and hardener into polymer composites [9–13]. Remendable polymers utilize thermally reversible reactions to repair a crack with some external intervention [14–16]. Hayes et al. [17, 18] have developed a two-phase, solid-state repairable polymer by dispersing a thermoplastic healing agent into the matrix of an E-glass/epoxy FRP. While the microcapsule-based and hollow-fiber-based self-healing systems demonstrate high healing efficiency, in general the healing is achievable only once for a given crack. Remendable systems are capable of multiple healing cycles, but require external intervention (heat or pressure). One strategy to extend the functional life of self-healing systems is to deliver a replenishable supply of the healing materials via a microvascular network [19, 20].

In a continuous self-healing system, shown schematically in Fig. 1, the matrix material contains embedded catalyst particles and interconnected microchannels for the storage and delivery of the healing agent. Similar to the microcapsule-based system [1], propagating cracks that intersect the microchannels cause healing agent to flow into the crack plane and react with the catalyst, healing the damage. The reopening of this crack after healing allows more healing agent to flow from the microchannels and heal the damage again. The large supply of healing agent is transported readily to the area of damage for multiple healing events. Recent analyses suggest ways to design and optimize vascularized networks for healing with minimized impact on structural performance [21–24]; the challenge is to realize these structures.

Advances in soft lithographic and direct-write assembly methods have enabled the creation of materials with complex embedded microvascular networks that emulate

K.S. Toohey · N.R. Sottos (✉, SEM Member) ·
S.R. White (SEM Member)
University of Illinois at Urbana-Champaign,
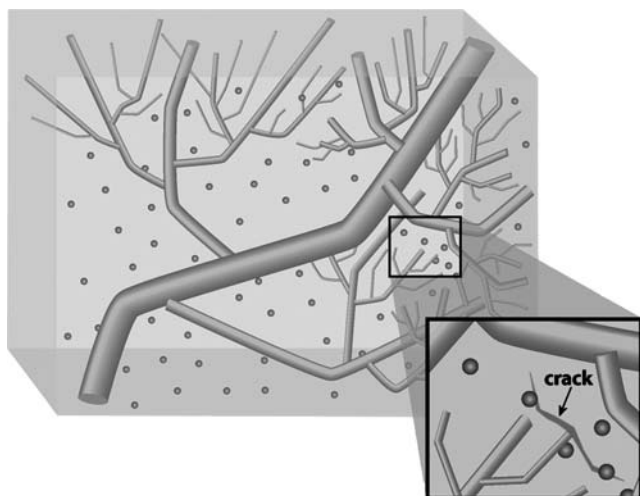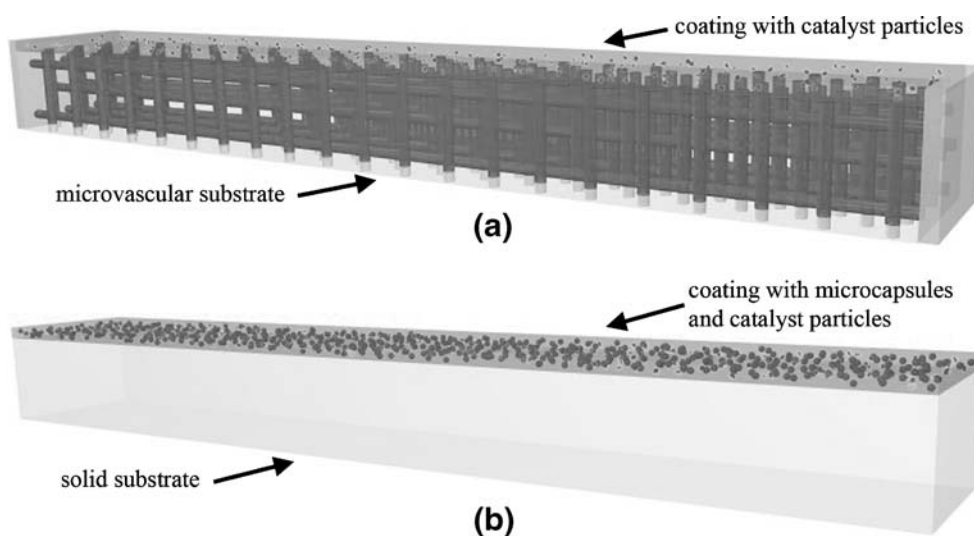Champaign, IL, USA
e-mail: n-sottos@uiuc.edu

Fig. 1 A schematic of the microvascular healing concept. A network of channels transports healing agent and catalyst particles are distributed throughout the matrix

many of the key responses of biological vascular systems [25–29]. In the current work, we incorporate pervasive microvascular networks in an epoxy matrix via direct-write assembly of an organic ink [25, 26]. Three-dimensional periodic scaffolds are fabricated by depositing the ink in a layer-by-layer build sequence followed by infiltration with an epoxy resin. The resin is then cured and the fugitive ink is subsequently removed under light vacuum by heating the structure to modest temperatures to liquefy the ink. The microvascular network has connections between the layers of channels everywhere that two ink lines are in contact in the scaffold.

In prior work on microencapsulated materials, the efficiency of crack healing is defined based on the ability of a healed sample to recover fracture toughness (K_{Ic}) [1, 3]. Fracture toughness is measured using a tapered double-cantilever beam (TDCB) test, which ensures controlled crack growth along the centerline of the brittle epoxy specimen. This TDCB specimen geometry is not well suited to evaluating the healing performance of microvascular networks and a new specimen design is required. Williams et al. [30] have developed a vascularized composite sandwich structure that is capable of healing a disbonded interface between the foam core and FRP laminate skin, resulting from impact damage. In the current work, we describe the testing protocol and analysis of a coated microvascular substrate specimen, shown in Fig. 2(a). A brittle epoxy coating is deposited on a more ductile substrate that contains a pervasive microvascular network. Solid catalyst particles are incorporated within the coating and the network is filled with a liquid healing agent. The coating/substrate beam is loaded in four-point bending until crack initiation occurs at the surface of the coating, where the tensile stress is maximum. A particularly desirable feature of the coating/substrate specimen geometry is that the cracks arrest at the coating interface and do not penetrate the more ductile microvascular substrate. The healing performance of the microvascular networks is compared with specimens containing microencapsulated healing agent and catalyst particles in the coating (but no microvascular network) as shown in Fig. 2(b). The microcapsule-filled coatings are effective in healing cracks in the coating, but not capable of rehealing a crack multiple times due to the limited local healing agent supply. In contrast, microvascular networks in the substrate are able to heal a crack for multiple cycles.

Materials and Methods

Healing Chemistry

A solid phase catalyst and a liquid monomer were combined in both the microcapsule and network specimens. Grubbs'

Fig. 2 Schematic of a self-healing (a) microvascular network specimen (b) microcapsule specimen

catalyst and dicyclopentadiene (DCPD) monomer, used successfully in microcapsule healing [1–8], were chosen for this study. Dicyclopentadiene has a low viscosity and can dissolve the Grubbs' catalyst quickly in the crack plane. In addition, the Grubbs' catalyst remains active during and after processing. The DCPD monomer and Grubbs' catalyst react by ring-opening metathesis polymerization (ROMP) to form a crosslinked polymer in the crack plane. Grubbs' catalyst is a living catalyst that remains active after polymerization, allowing for multiple healing events.

For the microcapsule-filled coatings, DCPD healing agent was encapsulated in a urea-formaldehyde shell using the process described by Brown et al. [31]. A solution containing urea, formaldehyde, and DCPD along with EMA (polyethylene-co-maleicanhydride), ammonium chloride, and resorcinol was heated to 55°C and stirred for 4 h. A stir rate of 900 rpm was used to form capsules that were 75–125 μm in diameter. Once the DPCD was encapsulated, the solution was filtered to remove the aqueous waste and the microcapsules were dried for 24 h at room temperature. The capsules were sifted to remove any remaining debris and to sort them by size.

Unprotected Grubbs' catalyst was dispersed in the coatings of both types of specimens. As-received Grubbs' catalyst (Sigma-Aldrich) was recrystallized to improve the dissolution of the catalyst in the healing agent, DCPD. This method is described in detail by Jones et al. [32]. In the coating, the crystals aggregated together to form larger particles averaging 150 μm in diameter.

Coating and Substrate Materials

The substrate for both beam types was made from a ductile epoxy (EnviroTex Lite, ETI, Inc.). This material was chosen for its reduced elastic modulus (2.5 GPa) and high strain to failure that enabled significant deflection when loaded in bending. As cracks developed in the brittle coating, the propagation stopped at the interface with the more ductile epoxy, preventing the failure of the entire specimen.

An epoxy coating with low strain to failure was chosen to facilitate cracking when applied to the more ductile substrate. For the coating, 12 parts per hundred (pph) diethylenetriamine (DETA) curing agent (Air Products) were mixed with EPON 828 resin (Miller Stephenson) and degassed. The microcapsules, wax beads, or unprotected Grubbs' catalyst particles were mixed into partially degassed polymer. Wax beads were used in the control beams as a nonreactive filler to take the place of the catalyst. The mixture was degassed again before pouring into the mold on the substrate. The brittle coatings were 500–800 μm thick, with an average thickness of approximately 700 μm, and the elastic modulus of the coating material was 3.5 GPa [19].

For specimens with microcapsule-filled coatings, solid beams of the Envirotex Lite epoxy were molded, cured, cut, and polished to be approximate 42–45 mm in length, 7–10 mm wide, and 5–7 mm high. A mold was placed around the edges of the substrate and the top of the substrate served as the bottom of the mold. The epoxy mixture with combinations of microcapsules, catalyst particles, and wax beads (with no catalyst) was poured into the mold on the top surface of the substrate. The coating was cured at room temperature for 24 h, and then was polished down to the desired thickness. The specimens were postcured at 25°C for an additional 24 h before testing.

Substrate beams with microvascular networks were fabricated via the direct write method described by Therriault et al. [26]. Three-dimensional scaffolds were drawn with a fugitive organic ink using a robotic controlled deposition (RCD) apparatus, that consisted of an ink delivery system mounted on a z-axis motion controlled stage for writing onto a moving x–y stage. A rectangular network with alternating layers of perpendicular channels was drawn by moving the x–y stage and extruding ink from the syringe with air pressure. After completion of each layer, the syringe was moved up in the z direction by 85% of the syringe diameter so that another layer could be drawn on top of the previous one. The center-to-center spacing between individual lines was ten times the diameter of the line. Consecutive layers were rotated by 90°, and every other layer was shifted by five times the diameter in-plane to create a face-centered tetragonal geometry. A 200 μm diameter tip was attached to a syringe containing the fugitive ink (60% petroleum jelly and 40% microcrystalline wax). The syringe was placed in a pressure-boosting device (HP7X, EFD, Inc.) that was fixed to the z-axis motion-controlled stage. The input air pressure was adjusted based on the room temperature and write speed to achieve the proper flow rate. Individual layers were deposited until the scaffold reached the desired height.

The ink structure was infiltrated with degassed EnviroTex Lite epoxy. The epoxy was cured, excess material was cut away, and the surfaces were polished. The final dimensions of the substrate were roughly 42–45 mm in length, 7–10 mm wide, and 5–7 mm high. The fugitive ink was removed by heating above the melt temperature of the ink (approximately 75°C) and applying a light vacuum. Channels were then rinsed five times with acetone by filling the network and removing the solvent with a light vacuum.

After the microvascular network was embedded into epoxy, the channels were blocked off by a polymer sealing the ends to prevent leakage of healing agent during testing. The channels were filled with an ultraviolet light-sensitive photopolymer (NOA 61, Norton Optical Adhesives). Opaque tape was used to mask the network so that approximately 1–2 mm along three edges (bottom, front

and back) were uncovered. Using a microscope with a mercury source ($\lambda=365$ nm), the edges were exposed to UV light to cure the polymer. The remaining uncured resin was removed with a vacuum and channels were rinsed continuously several times with acetone for 5-s periods until no more resin was removed from the channels.

Before the epoxy coating was applied to the microvascular network substrate, channels were filled with a fugitive wax (Purester 24, Strahl & Pitsch Inc.) to prevent the uncured coating material from penetrating the channels and partially blocking the network. The 828/DETA epoxy, with wax or catalyst, was molded on the top of the microvascular beam. The coatings for microvascular specimens were cured for a total of 48 h at 25°C. After the coating solidified, the network was heated to 35°C for approximately 10 min and the wax (melt temperature 25°C) was removed with a light vacuum. Channels were rinsed with acetone to ensure they were free of potential contaminants and DCPD monomer was placed in the channels using a syringe before testing. The channel ends remained unsealed during testing.

Test Protocol

The beams were loaded in four-point bending to place the coating in tension (Fig. 3). The lower span of the test fixture was 40 mm, the upper span was 20 mm, and the crosshead speed was 20 μm/s for initial tests (microcapsule beams) and increased to 50 μm/s for later tests (network beams). Load-displacement data was collected using Lab-VIEW (National Instruments) software. An acoustic emission (AE) sensor (model SE2MEG-P, Dunegan Engineering Company, Inc.) enabled detection of crack initiation or reopening during the tests. This sensor was necessary because the load drop associated with a crack reopening was not always apparent from the load-displacement plot.
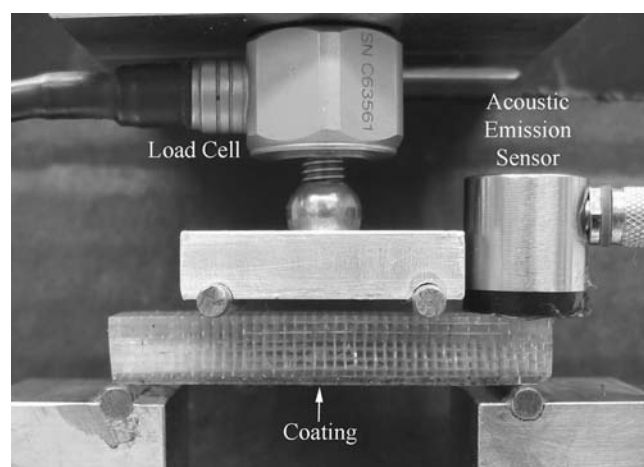

Fig. 3 Four-point bend test set-up with an acoustic emission sensor fixed to the specimen

The AE sensor was attached directly to the microvascular specimens using vacuum grease (Fig. 3), but was not used on the microcapsule filled specimens. Data from the AE sensor was collected with a digital oscilloscope (model LC584A, LeCroy) and was exported to a computer for comparison with the load-time data to determine the stress at which the first crack reopened.

An acoustic emission signal was used to determine the time of a crack formation or reopening event for the virgin and healed tests of the *in situ* microvascular specimens. In the virgin test, the formation of a crack resulted in a signal with high amplitude and many oscillations, as seen in Fig. 4(a). The reopening of a healed crack created a different signal than that of the virgin test. The signal for a crack that healed with high healing efficiency usually had a lower amplitude than the virgin and had fewer oscillations [Fig. 4(b)]. Cracks that did not heal well usually produced a weak AE signal with few oscillations [Fig. 4(c)]. When a crack did not heal at all, no AE signal was found. These signals were then used to determine the healing efficiency of each specimen for the various healing cycles tested.

A no-catalyst control test and an *in situ* healing test were performed for both the microvascular and the microcapsule beam specimens. Control specimens with no catalyst were tested to ensure no healing took place in the absence of catalyst. The self-healing and repeated self-healing capabilities were examined with *in situ* heal tests. For *in situ* coatings with microcapsules, only one combination of microcapsule concentration and catalyst concentration was studied, since this system has been well examined using the TDCB geometry [3]. The *in situ* coatings on specimens with microvascular networks contained varying concentrations of unprotected catalyst to study the effect of catalyst concentration on healing efficiency and number of possible healing cycles. Table 1 summarizes the different sample types tested.

Specimen Analysis

In a series of papers by Nairn and Kim [33–35], a finite fracture-mechanics model is developed to predict the formation of cracks in a thin coating on a substrate loaded in bending. The energy release rate due to the formation of each crack is determined using the stress in the coating, which is derived from a variational mechanics approach. Experimentally, the applied strain and crack density are fit to theoretical predictions to determine the critical energy release rate of the coating *in situ*.

To begin the analysis, the substrate is divided into two regions with thicknesses, t_2 and t_3, and the coating has thickness t_1. The strain energy for a single crack interval is found and then differentiated to find the mechanical energy

Fig. 4 Representative acoustic emission signals for (**a**) the formation ▶ of a virgin crack, (**b**) the reopening of a well healed crack, and (**c**) the reopening of a poorly healed crack

(a)

(b)

(c)

release rate. The energy release rate for the first crack to occur in the coating is

$$G = C_3 t_1 \left\langle \sigma_{xx,m0}^{(1)} \right\rangle^2 \lim_{D \to 0} Y(D) \tag{1}$$

where C_3 and $\lim_{D \to 0} Y(D)$, a function of the crack density (D), are found through a variational mechanics analysis. The average initial mechanical stress before fracture, $\left\langle \sigma_{xx,m0}^{(1)} \right\rangle$, is calculated from experimental data using beam theory as described in the Appendix. The expressions for C_3 and $\lim_{D \to 0} Y(D)$ are derived in papers by Nairn and Kim [33, 35]. For the experiments conducted in this work, the fracture toughness of the initial crack in the coating is calculated using the peak stress when fracture occurs in both the virgin and healing tests.

The energy release rate is used to determine the healing efficiency based on the fracture toughness of the virgin and healed tests. Mode I fracture toughness, K_{Ic}, is related to energy release rate [36] by

$$K_{Ic} = \sqrt{GE}. \tag{2}$$

The ratio of fracture toughness of the healed material and the virgin material is an established measure of crack repair in polymers [37–40]. Healing efficiency, as defined by White et al. [1] is

$$\eta = \frac{K_{Ic}^{healed}}{K_{Ic}^{virgin}}. \tag{3}$$

From equations (1) and (2) and the analysis in the Appendix, the fracture toughness is directly proportional to the applied load, reducing the healing efficiency calculation to

$$\eta = \frac{P^{healed}}{P^{virgin}}. \tag{4}$$

Results and Discussion

Bending tests were performed for all of the coating/substrate specimens listed in Table 1. Representative load-time plots for the control tests and *in situ* healing tests of both microcapsule and network beam specimens are shown in Figs. 5 and 6. Multiple cracks in the coating were allowed to form in microcapsule-filled coatings. The fracture toughness value for the microcapsule specimens were calculated using the load at the formation of the first crack. In order to isolate the repeated healing in the
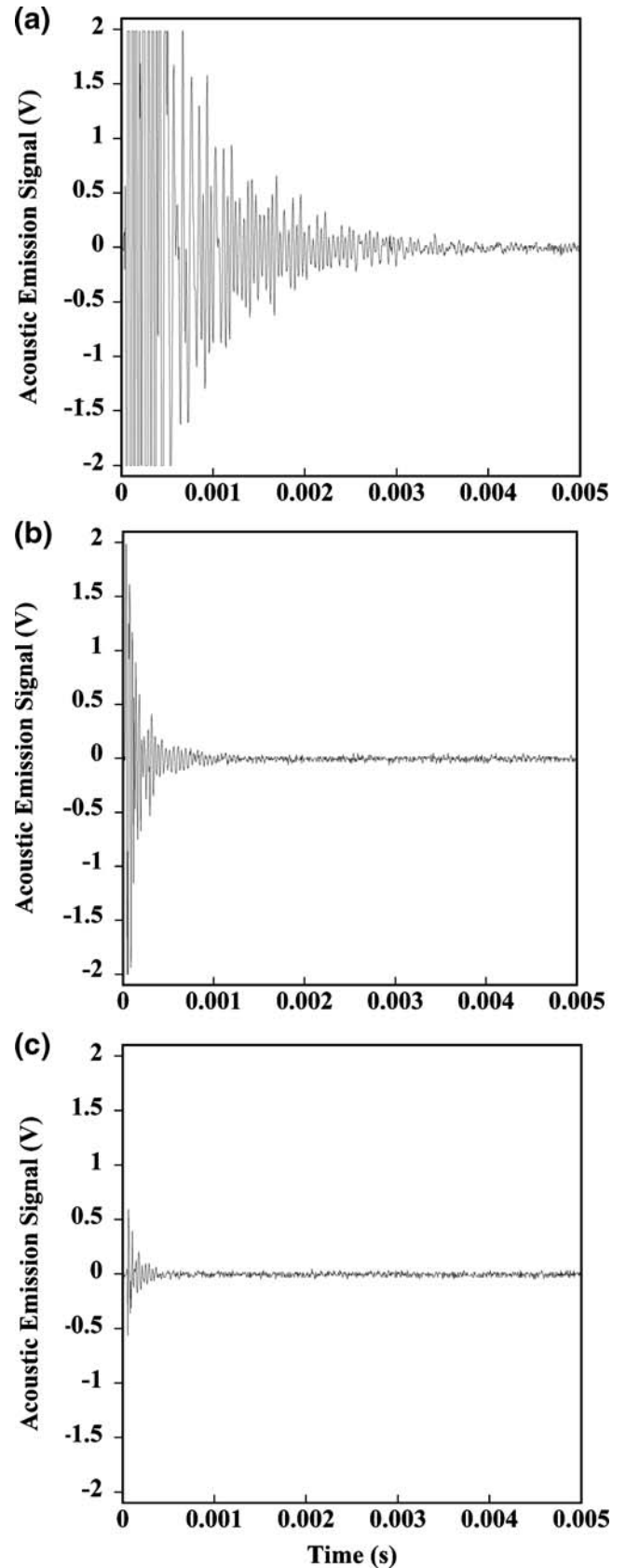
Table 1 Concentration of self-healing components in microcapsule and microvascular specimens

	Coating	
	Capsules (wt.%)	Catalyst (wt.%)
Capsule control	10	0
Capsule in situ	10	2
Network control	0	0
Network in situ	0	2, 5 or 10

microvascular network specimens, the coatings were allowed only a single crack in the virgin test. Loading was stopped immediately after the crack formation and the same crack was reopened in the subsequent healing tests.

Microcapsule Beams

Control specimens containing 5 wt.% DCPD filled capsules and 10 wt.% wax beads with 0 wt.% catalyst were loaded in bending to form cracks in the coating. After resting for 48 h at room temperature, specimens were reloaded to confirm that no healing occurred. DPCD healing agent was observed in the crack plane confirming the rupture of the microcapsules. During reloading, the unbonded crack faces reopened immediately with no audible sound confirming that no healing took place.

An examination of the fracture surface by scanning electron microscopy (SEM) after the reloading test confirmed that no healing occurred for this control specimen. The fracture plane had no evidence of a polymerized film on the surface anywhere along the length of the crack. Figure 7(a) shows the fracture surface after the heal period for a no-catalyst crack.

In situ coatings with 2 wt.% unprotected catalyst and 10 wt.% microcapsules were examined for their self-healing capabilities. After crack formation in the virgin test, specimens healed at room temperature for 48 h before retesting. Upon reloading, the cracks in the coatings remained bonded together at low load, and when the critical stress in the coating was reached, all of the cracks reopened audibly. The average healing efficiency for the microcapsule-filled *in situ* coatings was 49% for six specimens. All of these specimens only healed for one cycle.

Microcapsule-filled coatings with catalyst demonstrated healing efficiencies comparable to those measured with TDCB fracture specimens [3]. Upon inspection of the coatings under SEM, poly(DCPD) films were apparent across most of the crack plane. The two sides of a single crack in a coating with 2 wt.% catalyst and 10 wt.% microcapsules are shown in Fig. 8. The polymerized film on the two surfaces indicates a large area of coverage in the crack plane.

Microvascular Beams

Control specimens containing no catalyst were tested to ensure that no healing of the cracks occurred without a polymerizing agent. The coatings for this control test contained 10 wt.% wax beads (with no catalyst). After the initial formation of a crack, DCPD monomer flowed from the channels to the crack. During the 48-h rest period, the monomer evaporated, leaving the crack plane unhealed. The recovery of fracture toughness of all five specimens was 0%, because the cracks in the coatings reopened immediately upon reloading the beams.

The absence of a polymerized film on the crack plane was confirmed through examination of the crack surfaces with SEM. Figure 7(b) shows the virgin fracture surface of a specimen with no catalyst. Many wax beads were visible on the surface, but there was no evidence of healing.

Fig. 5 Typical load-time plots for (**a**) a no-catalyst, microcapsule specimen, (**b**) an *in situ* microcapsule specimen with 40% healing efficiency. The loading rate for both tests was 20 μm/s. The second loading traces in each plot were shifted by 1 s in order to visualize the data sets individually

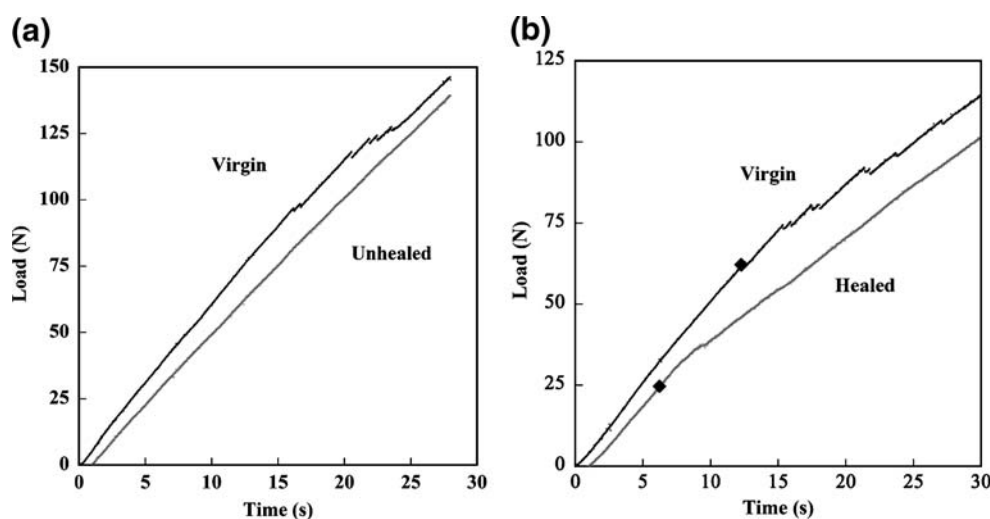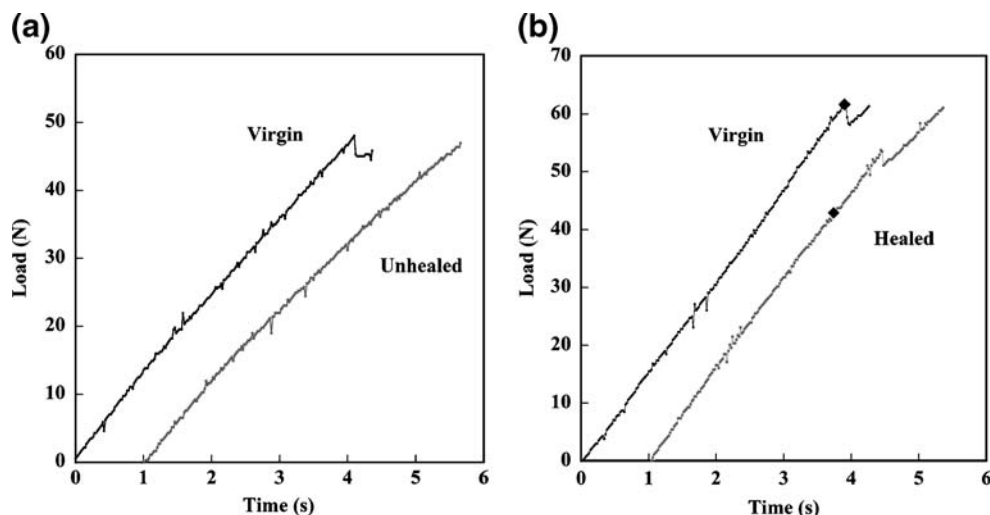**Fig. 6** Typical load-time plots for (**a**) a no-catalyst, network specimen, (**b**) an *in situ* network specimen. The loading rate for both tests was 50 μm/s. The second loading traces in were shifted by 1 s in order to visualize the data sets individually

For the *in situ* tests, microvascular substrates were prepared and coatings with unprotected catalyst (2%, 5% or 10% by weight) were applied similarly to the coatings with unprotected catalyst. Monomer was flowed into the networks using a syringe and the virgin tests were performed. After testing, the fluid was removed using light vacuum pressure, and specimens were healed at 25°C for 12 h. Networks were recharged with monomer and the heal tests were performed. This cycle was repeated eight times for all specimens.

Microvascular specimens with unprotected catalyst in the coating achieved multiple healing cycles for a single crack in a coating. Figure 6(b) shows the virgin and second heal cycle load data for a specimen with 10 wt.% catalyst in the coating. The critical crack opening events, from the AE data, are indicated by the large black squares on each data set. The loads of these crack opening events were used in the calculation of the healing efficiency. This specimen [Fig. 6(b)] performed the best of all specimens tested,

healing seven times with an average healing efficiency of 51%. The eighth cycle showed no healing.

Average healing efficiencies relative to the healing of the microcapsule beams for sets of network specimens with 2%, 5% and 10% catalyst by weight are shown in Fig. 9. A minimum of six specimens were tested for each concentration of catalyst. Because of additional cracking or inconclusive AE data, several specimens from each set were excluded. The maximum healing efficiency for most specimens was in the second healing cycle. The concentration of catalyst in the coating did not significantly affect the average healing efficiency for each cycle, but did influence the number of healing cycles possible. The average number of heals was 2, 2, and 4 for coatings with 2%, 5%, and 10% catalyst by weight, respectively. Although improved healing is achieved with high catalyst concentrations, these
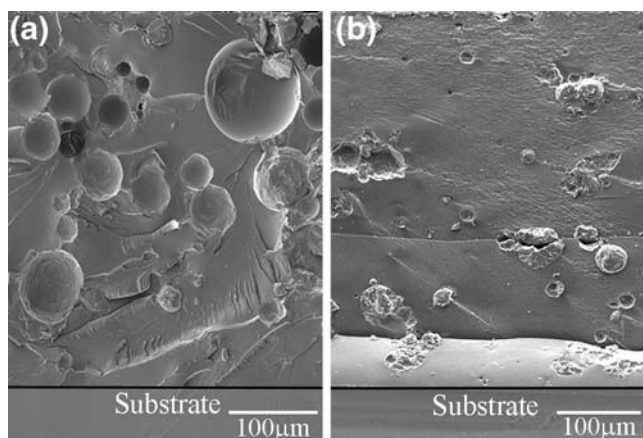

Fig. 7 Scanning electron micrographs of unhealed crack surfaces. (**a**) A crack in a coating with microcapsules and no catalyst, and (**b**) a crack in a coating with wax beads on a microvascular substrate
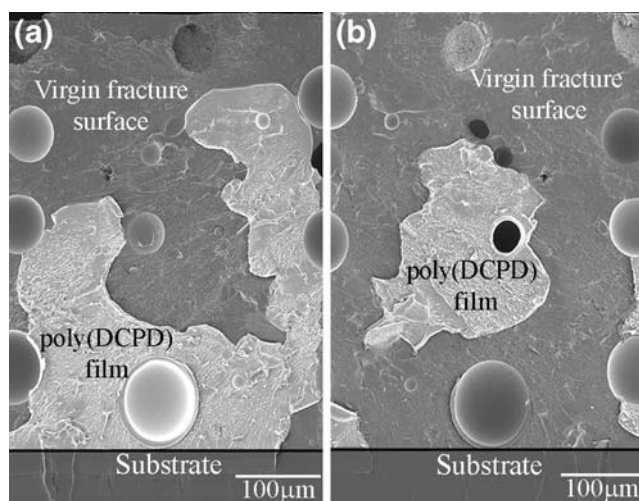

Fig. 8 Scanning electron micrographs of a self-healing coating containing microcapsules. (**a**) One side of a crack with healed poly (DCPD) film on the surface and (**b**) the opposite face of the same crack with corresponding healed surfaces
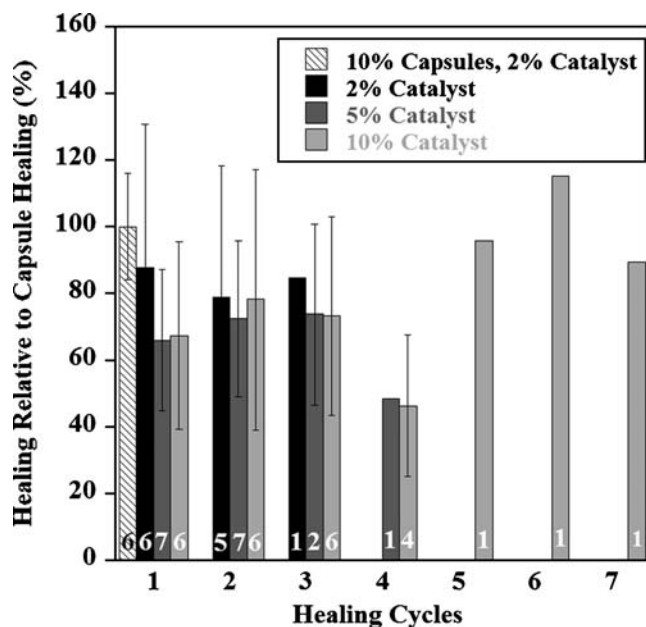
Fig. 9 Healing efficiency relative to the healing of microcapsules beams. The number in each column indicates the number of specimens tested in the average healing value

concentrations can reduce the virgin fracture toughness of the coating [3].

Evidence of polymerized material was visible on the crack planes with SEM for the *in situ* network specimens. The amount of material on the crack plane was determined by the concentration of catalyst in the coating and the number of successful healing cycles achieved by the crack. The micrograph in Fig. 10(a) reveals small areas of poly (DCPD) on the crack face, but most of the crack was
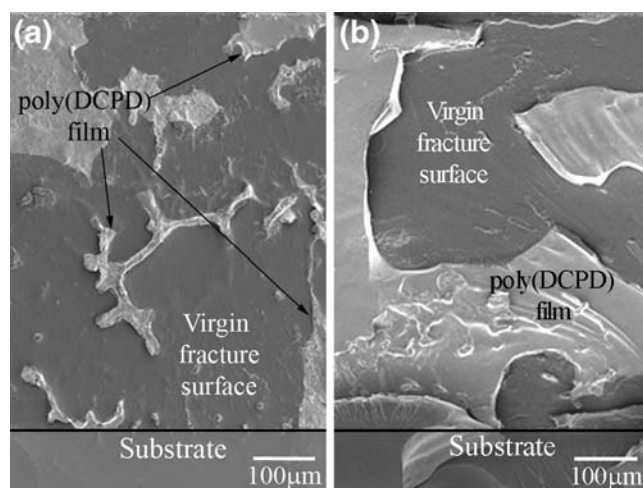

Fig. 10 Scanning electron micrograph of cracks that healed in a coating with 5 wt.% catalyst. (a) A crack that healed for a single cycle shows poor coverage of the poly(DCPD) film, and (b) a crack that healed four cycles has larger regions with poly(DCPD) healed film on the surface
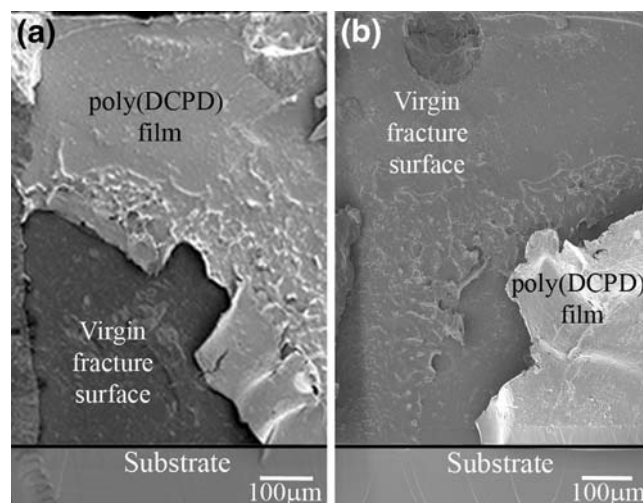

Fig. 11 A scanning electron micrograph of two sides of a crack face that healed for seven cycles in a coating with 10% catalyst. The crack face in this area is completely covered by polymerized DCPD
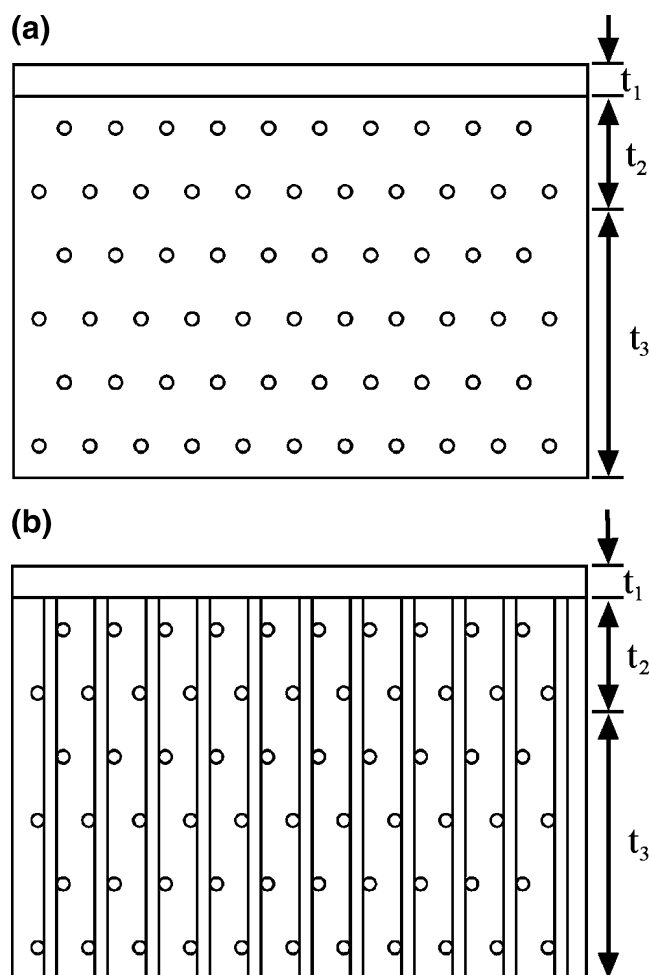

Fig. 12 Two cross sections of network beams with (a) out-of-plane channels, and (b) in-plane and out-of-plane channels

unhealed in this coating with 5 wt.% catalyst that healed for one cycle. Incomplete coverage of the crack by a polymerized film was typical of specimens with 2 wt.% and 5 wt.% catalyst that healed for one or two cycles. In contrast, the fracture surfaces of a specimen with 10 wt.% catalyst that healed seven times (Fig. 11) shows large areas of poly(DCPD) coverage on both sides of the crack face. The fracture surface of another specimen containing 5 wt.% catalyst [Fig. 10(b)] demonstrates that more successful healing cycles increases the coverage of polymerized film on the crack planes. Large areas of polymerized film on the crack faces were common in specimens with 5 wt.% or 10 wt.% catalyst that healed for many cycles. Often when a crack intersected larger catalyst particles, good film coverage was seen in the region surrounding the catalyst.

Ideally, the microvascular samples should reheal the same crack indefinitely, given a renewable supply of healing agent. A maximum of seven healing cycles was achieved for a coating on a substrate with a microvascular network. Due to variations in the size and distribution of the catalyst particles, the number of healing cycles achieved by a single crack varied. In specimens where the crack intersected a large catalyst particle, generally more healing cycles were possible. A similar trend was seen in the sets of specimens with different concentrations of catalyst. Higher concentrations of Grubbs' catalyst in the coating lead to more healing cycles in the network specimens with unprotected catalyst.

Reactive Grubbs' catalyst was essential for each successful healing cycle. Even though it is considered a living catalyst, the mobility of the Grubbs' catalyst at the active ends of the poly(DCPD) chains was greatly restricted after healing. The solid polymer that was formed by the ROMP reaction between DCPD monomer and Grubbs' catalyst effectively consumed the catalyst with each healing cycle. After the local supply in the crack plane was exhausted, the healing efficiency dropped to zero.

Conclusions

A new protocol was developed to assess the ability to heal a brittle coating applied on a ductile substrate. The coating/substrate specimen geometry was particularly well suited to examine the healing performance of substrates with an embedded microvascular networks. Beam specimens were loaded in four-point bending to initiate and reopen cracks in the coatings in virgin and healed tests. The use of an acoustic emission sensor during tests enabled the detection crack opening and reopening to determine the critical loads of these events. Using the loads of crack opening and reopening, a reliable measure of crack healing in brittle coatings was established.

Tests of beams with self-healing brittle coatings confirmed that the microcapsule-based healing system was only capable of a single healing cycle, while the network-based healing system healed a single crack for up to seven cycles. The microcapsules-filled coatings achieve and average healing efficiency of 49%, while the microvascular substrate specimens were capable of 38% healing efficiency on average for all catalyst concentrations. Higher concentrations of catalyst in the coating for microvascular beams generally increased the number of healing cycles possible for a single crack. The only limitation of the number of healing cycles was the finite supply of catalyst in the coating, which was effectively consumed with each healing event.

Appendix

The two types of specimen were tested in four-point bending to create cracks in the brittle coating. The outer and inner support spans for the bend tests were $A=40$ mm and $B=20$ mm, respectively. Assuming the load is distributed equally among the four supports, the bending moment between the inner supports is therefore constant and depends on the load P and span distances according to the relation,

$$M = \frac{1}{4}P(A - B) \tag{5}$$

The axial stress in the coating is then calculated by

$$\sigma = \frac{My}{I_{\text{composite}}}, \tag{6}$$

where $I_{\text{composite}}$ is the composite moment of inertia and y is the distance from the neutral axis.

The microcapsule beams are comprised of two materials with different elastic properties. The elastic modulus of the coating is approximately 1.4 times that of the substrate (3.5 GPa and 2.5 GPa, respectively). The difference in stiffness of the two materials leads to a more complicated stress calculation. A factor of 1.4 is introduced in the calculation for the coating moment of inertia, I_c, to account for the difference in the elastic moduli of the two materials:

$$I_s = \frac{1}{12}bh^3, \ I_c = \frac{1.4}{12}bt^3. \tag{7}$$

The subscripts s and c refer to properties of the substrate and coating, respectively. The composite centroid of the

microcapsule beam, $y_{capsule}$, and the moment of inertia of the composite are calculated,

$$y_{capsule} = \frac{A_s y_s + A_c y_c}{A_s + A_c}, \tag{8}$$

$$I_{capsule} = I_s + A_s d_s^2 + I_c + A_c d_c^2, \tag{9}$$

where A is the area of the individual sections, y is the distance to the centroid of each area from the base. The distance, d, between each individual centroid and the composite centroid is given by

$$A_s = bh, \; A_s = 1.4bt, \tag{10}$$

$$y_s = h/2, \; y_s = h + t/2, \tag{11}$$

$$d_i = y_{capsule} - y_i. \tag{12}$$

Adding a microvascular network to the substrate changes the effective cross-sectional area and therefore changes the moment of inertia of the beam. Because the cross sections of the network beam vary depending on the location along the beam, a rule-of-mixtures approach is used to calculate the corresponding moment of inertia. Two cross sections are shown in Fig. 12(a) one with no vertical channels and Fig. 12(b) the other with maximum-diameter vertical channels. The centroid of cross section (b) is assumed equal to that of (a). The difference between the centroidal positions of the two sections is negligible for thin coatings in which the height of the vertical channels is approximately equal to the height of the total cross section. The composite centroid of (a) is found and then used to calculate the composite moment of inertia for both cross sections:

$$y_{net} = \frac{A_s y_s + A_c y_c - \sum A_{h1_i} y_{h1_i}}{A_s + A_c - \sum A_{h1_i}}, \tag{13}$$

$$I_{net1} = I_s + A_s d_s^2 + I_c + A_c d_c^2 - \sum \left(I_{h1} + A d_{h1}^2 \right), \tag{14}$$

$$I_{net2} = I_s + A_s d_s^2 + I_c + A_c d_c^2 - \sum \left(I_{h1} + A d_{h1}^2 \right) \\ - \sum I_{h2} + 2rh d_{h2}^2. \tag{15}$$

The new subscripts, $h1$ and $h2$, refer to out-of-plane and in-plane channels, respectively, and r is the radius of the channels. The area of the out-of-plane channels in the cross section is $A = \pi r^2$. The locations of the out-of-plane channels (y_{h1}) are determined by the spacing between channels, and

the location of the in-plane channels is $y = h/2$. The areas, moments of inertia, and distances y and d for the coating and substrate are previously defined. Because the spacing between the centerline of the channels is five times the diameter of the channels, the approximate ratio of cross sections with and without the in-plane channels is 1:4. By the rule of mixtures, 80% of the beam has I_{net1} for the moment of inertia and 20% has I_{net2}, or

$$I_{network} = 0.8 I_{net1} + 0.2 I_{net2}. \tag{16}$$

References

1. White SR, Sottos NR, Geubelle PH, Moore JS, Kessler MR, Sriram SR et al (2001) Autonomic healing of polymer composites. Nature 409:794–797. doi:10.1038/35057232
2. Rule JD, Brown EN, Sottos NR, White SR, Moore JS (2005) Wax-protected catalyst microspheres for efficient self-healing. Adv Mater 172:205–208. doi:10.1002/adma.200400607
3. Brown EN, Sottos NR, White SR (2002) Fracture testing of a self-healing polymer composite. Exp Mech 424:372–379. doi:10.1007/BF02412141
4. Brown EN, White SR, Sottos NR (2004) Microcapsule induced toughening in a self-healing polymer composite. J Mater Sci 39:1703–1710. doi:10.1023/B:JMSC.0000016173.73733.dc
5. Brown EN, White SR, Sottos NR (2006) Fatigue crack propagation in microcapsule toughened epoxy. J Mater Sci 41:6266–6273. doi:10.1007/s10853-006-0512-y
6. Brown EN, White SR, Sottos NR (2005) Retardation and repair of fatigue cracks in a microcapsule toughened epoxy composite—part 1: manual infiltration. Compos Sci Technol 65:2466–2473. doi:10.1016/j.compscitech.2005.04.020
7. Brown EN, White SR, Sottos NR (2005) Retardation and repair of fatigue cracks in a microcapsule toughened epoxy composite—part 2: in situ self-healing. Compos Sci Technol 65:2474–2480. doi:10.1016/j.compscitech.2005.04.053
8. Kessler MR, Sottos NR, White SR (2003) Self-healing structural composite materials. Compos Part A 34:743–753. doi:10.1016/S1359-835X(03)00138-6
9. Dry C (1996) Procedures developed for self-repair of polymer matrix composite materials. Compos Struct 35:263–269. doi:10.1016/0263-8223(96)00033-5
10. Pang JWC, Bond IP (2005) 'Bleeding composites'—enhanced damage detection and self repair using a biomimetic approach. Compos Part A 36:183–188
11. Pang JWC, Bond IP (2005) A hollow fibre reinforced polymer composite encompassing self-healing and enhanced damage visibility. Compos Sci Technol 65:1791–1799. doi:10.1016/j.compscitech.2005.03.008
12. Trask RS, Williams GJ, Bond IP (2007) Bioinspired self-healing of advanced composite structures using hollow glass fibres. J R Soc Interface 4:363–371. doi:10.1098/rsif.2006.0194
13. Trask RS, Bond IP (2006) Biomimetic self-healing of advanced composite structures using hollow glass fibres. Smart Mater Struct 15:704–710. doi:10.1088/0964-1726/15/3/005
14. Chen X, Dam MA, Ono K, Mal A, Shen H, Nutt SR et al (2002) A thermally re-mendable cross-linked polymeric material. Science 295:1698–1702. doi:10.1126/science.1065879
15. Chen X, Wudl F, Mal AK, Shen H, Nutt SR (2003) New thermally remendable highly cross-linked polymeric materials. Macromolecules 36:1802–1807. doi:10.1021/ma0210675

16. Kalista SJ Jr, Ward TC (2007) Thermal characteristics of the self-healing response in poly(ethylene-co-methacrylic acid) copolymers. J R Soc Interface 4:405–411. doi:10.1098/rsif.2006.0169

17. Hayes SA, Jones FR, Marshiya K, Zhang W (2007) A self-healing thermosetting composite material. Compos Part A 384:1116–1120. doi:10.1016/j.compositesa.2006.06.008

18. Hayes SA, Zhang W, Branthwaite M, Jones FR (2007) Self-healing of damage in fibre-reinforced polymer-matrix composites. J R Soc Interface 413:381–387. doi:10.1098/rsif.2006.0209

19. Toohey KS (2007) Microvascular networks for continuous self-healing materials. Ph.D. thesis, Department of Mechanical Science and Engineering, University of Illinois at Urbana-Champaign

20. Toohey KS, Sottos NR, Lewis JA, Moore JS, White SR (2007) Self-healing materials with microvascular networks. Nat Mater 68:581–585. doi:10.1038/nmat1934

21. Aragón AM, Hansen CJ, Wu W, Geubelle PH, Lewis JA, White SR (2007) Computational design and optimization of a biomimetic self-healing/cooling material. In: Dapino MJ (ed) Proceedings of SPIE, vol 6526. SPIE, Bellingham, WA, p 65261G

22. Kim S, Lorente S, Bejan A (2006) Vascularized materials: tree-shaped flow architectures matched canopy to canopy. J Appl Phys 1008:063525. doi:10.1063/1.2349479

23. Williams HR, Trask RS, Knights AC, Williams ER, Bond IP (2008) Biomimetic reliability strategies for self-healing vascular networks in engineering materials. J R Soc Interface 524:735–747. doi:10.1098/rsif.2007.1251

24. Williams HR, Trask RS, Weaver PM, Bond IP (2008) Minimum mass vascular networks in multifunctional materials. J R Soc Interface 518:55–65. doi:10.1098/rsif.2007.1022

25. Therriault D (2003) Directed assembly of three-dimensional microvascular networks. Ph.D. thesis, Department of Aerospace Engineering, University of Illinois at Urbana-Champaign

26. Therriault D, White SR, Lewis JA (2003) Chaotic mixing in three-dimensional microvascular networks fabricated by direct-write assembly. Nat Mater 24:265–271. doi:10.1038/nmat863

27. Runyon MK, Johnson-Kerner BL, Ismagilov RF (2004) Minimal functional models of hemostasis in a biomimetic microfluidic system. Angew Chem Int Ed 43:1531–1536. doi:10.1002/anie.200353428

28. Stroock AD, Cabodi M (2006) Microfluidic biomaterials. MRS Bull 31:114–119

29. Lim D, Kamotani Y, Cho B, Mazumder J, Takayama S (2003) Fabrication of microfluidic mixers and artificial vasculatures using a high-brightness diode-pumped Nd:YAG laser direct write method. Lab Chip 3:318–323. doi:10.1039/b308452c

30. Williams HR, Trask RS, Bond IP (2007) Self-healing composite sandwich structures. Smart Mater Struct 164:1198–1207. doi:10.1088/0964-1726/16/4/031

31. Brown EN, Kessler MR, Sottos NR, White SR (2003) In situ poly (ureaformaldehyde) microencapsulation of dicyclepentadiene. J Microencapsul 206:719–730. doi:10.1080/0265204031000154160

32. Jones AS, Rule JD, Moore JS, White SR, Sottos NR (2006) Catalyst morphology and dissolution kinetics for self-healing polymers. Chem Mater 18:1312–1317. doi:10.1021/cm051864s

33. Kim S-R, Nairn JA (2000) Fracture mechanics analysis of coating/substrate systems Part I: analysis of tensile and bending experiments. Eng Fract Mech 65:573–593. doi:10.1016/S0013-7944(99)00141-1

34. Kim S-R, Nairn JA (2000) Fracture mechanics analysis of coating/substrate systems part II: experiments in bending. Eng Fract Mech 65:595–607. doi:10.1016/S0013-7944(99)00142-3

35. Nairn JA, Kim S-R (1992) A fracture mechanics analysis of multiple cracking in coatings. Eng Fract Mech 421:195–208. doi:10.1016/0013-7944(92)90291-L

36. Anderson TL (1995) Fracture mechanics fundamentals and applications, 2nd edn. CRC, New York, NY

37. Wool RP, O'Connor KM (1982) A theory of crack healing in polymers. J Appl Phys 52:5953–5963. doi:10.1063/1.328526

38. Jud K, Kausch HH, Williams JG (1981) Fracture mechanics studies of crack healing and welding of polymers. J Mater Sci 16:204–210. doi:10.1007/BF00552073

39. Kausch HH, Jud K (1982) Molecular aspects of crack formation and healing in glassy polymers. Plast Rubber Process Appl 2:265–268

40. Wang EP, Lee S, Harmon J (1994) Ethanol-induced crack healing in poly(methyl methacrylate). J Polym Sci B Polym Lett 32:1217–1227